


Onset of nonequilibrium in a driven Anderson insulatorZ. Ovadyahu *Racah Institute of Physics, The Hebrew University, Jerusalem 9190401, Israel*

(Received 24 May 2023; accepted 12 December 2023; published 27 December 2023)

The onset of nonequilibrium in a driven Anderson insulator is identified by monitoring the system with two thermometers. Features of nonequilibrium appear at surprisingly weak drive intensity demonstrating, among other things, that conductivity may not be a reliable thermometer for ensuring linear-response conditions. In addition, the spectral contents of the applied field could be more important to take the system out of equilibrium than its absorbed power. Ensuing hot-electron transport effects and the nontrivial role phonons play in driven quantum systems are pointed out.

DOI: [10.1103/PhysRevB.108.L220203](https://doi.org/10.1103/PhysRevB.108.L220203)

Below 1K, you know the temperature if you have one thermometer; when you have two, you don't. This adage is recalled whenever a sample resistance fails to follow the expected dependence on temperature given by the fridge-installed thermometer. Such an event is often related to an influx of energy causing a lack of detailed balance with the bath. The sample may still be in a steady state but not in thermal equilibrium. Considerable attention has been given to nonequilibrium states, created by a variety of means, to look for novel phenomena [1–6]. A nonequilibrium steady state (NESS) is a common occurrence in low temperature transport experiments making it a natural testbed for these studies.

Monte Carlo simulations of driven disordered systems supported the intuitive notion that the electrons may be assigned an effective temperature T_{eff} distinctly different from the phonon temperature [7,8]. The effective temperature of the electrons was defined by fitting their energy distribution to the Fermi-Dirac expression [7,8]. The relevance of an effective temperature under drive by external fields is one of the issues tested experimentally here.

In this Letter, we outline a method to detect the onset of nonequilibrium in a driven electronic system by comparing the readings of two thermometers. These are attached to the electronic conductance of an interacting Anderson insulator, also known as the electron glass [9–17]. Once driven by external fields, both thermometers read higher temperatures than that of the bath. As the drive power increases from the lowest level of the experiment, they exhibit different T_{eff} 's, signaling a breakaway from thermal equilibrium. The difference between the two thermometers' readings, ΔT_{eff} , increases monotonously with the drive intensity. Significantly, ΔT_{eff} turns out to be sensitive to the spectral contents of the energy supplied by the drive, not just its magnitude. The results shed further light on the glassy nature of the Anderson insulating phase and, in particular, on the reason for its sluggish dynamics in relation to the much faster transitions involved in the conductance.

Samples used in this study were 20 nm thick films of amorphous indium oxide (In_xO). These were made by e-gun evaporation of 99.999% pure In_2O_3 onto room-temperature Si wafers in a partial pressure of 3×10^{-4} mBar of O_2 and

a rate of $0.3 \pm 0.1 \text{ \AA/s}$. The Si wafers (boron doped with bulk resistivity $\rho \leq 2 \times 10^{-3} \text{ \Omega cm}$) were employed as the gate electrode in the field effect and experiments. The samples were deposited on a SiO_2 layer (2 μm thick) that was thermally grown on these wafers and acted as the spacer between the sample and the conducting Si:B substrate. The carrier concentration N of these samples, measured by the Hall effect at room temperatures, yielded carrier concentration $N \approx (1 \pm 0.4) \times 10^{19} \text{ cm}^{-3}$. There are to date six Anderson insulators that may be used for these experiments [18]. The motivation for choosing this version of In_xO was its highly pronounced memory dip, which is used here as a sensitive thermometer.

Conductivity of the samples was measured using a two-terminal ac technique employing a 1211-ITHACO current preamplifier and a PAR-124A lock-in amplifier. Measurements were performed with the samples immersed in liquid helium at $T \approx 4.1 \text{ K}$ held by a 100 liters storage dewar. This allowed up to two months measurements on a given sample while keeping it cold. These conditions are essential for measurements where extended times of relaxation processes are required at a constant temperature, especially when running multiple excitation-relaxation experiments on a given sample. The gate-sample voltage (referred to as V_g in this work) in the field-effect measurements was controlled by the potential difference across a 10 μF capacitor charged with a constant current. The rate of change of V_g is determined by the value of this current. Except when otherwise noted, the ac voltage bias used in conductivity measurements was small enough to ensure near-ohmic conditions. Exciting the system by infrared radiation was accomplished by a light-emitting AlGaAs diode operating at $\approx 0.85 \pm 0.05 \text{ \mu m}$. It was placed $\approx 15 \text{ mm}$ from and facing the sample surface. The thermometers used for the study are two distinct properties of electron glasses: the conductance G and its sensitivity to a change of the carrier concentration N . The latter was affected by changing the voltage V_g between the sample and a nearby gate electrode. A typical field-effect measurement using this MOSFET configuration is shown in Fig. 1. The figure also illustrates how the parameters G_0 and G_1 , used for determining the temperature of the two thermometers, are defined. The first thermometer

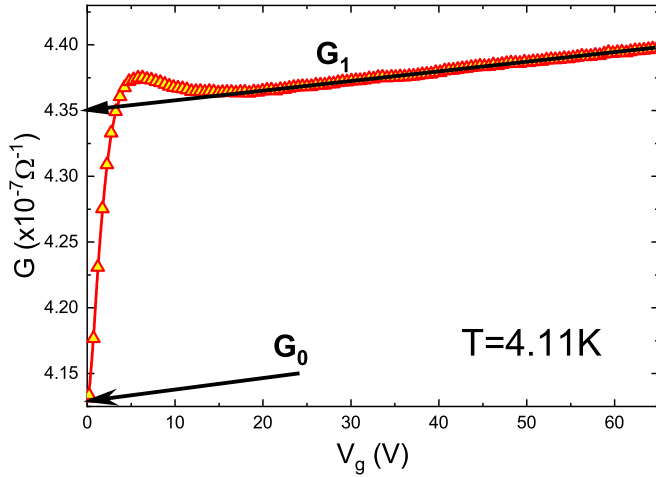


FIG. 1. Conductance vs gate voltage V_g for a 20 nm thick In_xO film with 1 mm \times 1 mm lateral size. Data were taken with a sweep rate $\partial V_g/\partial t$ of 1.2 V/s at a bath temperature $T = 4.11$ K. The values of the two parameters used in the text, G_0 and G_1 , are taken as the intercepts of the arrows with the ordinate. The “bump” at $V_g \approx 6$ V is a consequence of charge ordering as explained in [19].

reading is the steady-state conductance $G_0 = G(V_g = 0)$. The second thermometer reading is $\eta = (G_1 - G_0)/G_0$, where G_1 is determined by the construction in Fig. 1. The same sweep rate $\partial V_g/\partial t = 1.2$ V/s was used in all $G(V_g)$ traces in this work. Note that the need to complete the $G(V_g)$ trace makes the second thermometer “slower” than the first, a difference that plays a role in their response. Both G_0 and η turn out to be strongly temperature dependent, making them sensitive “secondary” thermometers. Applying them for temperature measurements requires calibration charts for each. These are shown in Figs. 2 and 3 for $G_0(T)$ and $\eta(T)$, respectively.

Figure 4 shows a set of $G(V_g)$ curves taken by using non-Ohmic fields to measure both the sample conductance and its associated field effect. All other aspects of the measurements protocol were identical to those used in obtaining the data set in Fig. 3.

Evidently, the two sets shown in Figs. 3 and 4 bear strong resemblance to one another. The conditions under which these data were collected, however, are quite different; the set in Fig. 3 was taken at equilibrium, while that in Fig. 4 was taken as a NESS. The similarity in terms of how the $G(V_g)$ curves evolve with either temperature or field may tempt one to assign a T_{eff} for a given $G(F)$. At the same time, an effective temperature $T_{\text{eff}}(F)$ may be independently inferred from the data sets in Fig. 2 based on G_0 . These two protocols for assigning a $T_{\text{eff}}(F)$ use the *same* set of measurements while focusing on different parts of the $G(V_g, F)$ data. They yield, however, quite different values for T_{eff} as is shown in Figs. 5 and 6 below.

Figure 5 compares a set of η 's measured at *equilibrium* temperatures with the set measured under NESS conditions produced by applying different fields. The latter is plotted versus T_{eff} calibrated against the data in Fig. 2(b) on the basis of G_0 values. For brevity's sake, we shall refer to this set of $T_{\text{eff}}(F)$ as that of thermometer 1. $T_{\text{eff}}(F)$ for thermometer 2 is then obtained by finding the temperature on the $\eta(T)$ curve

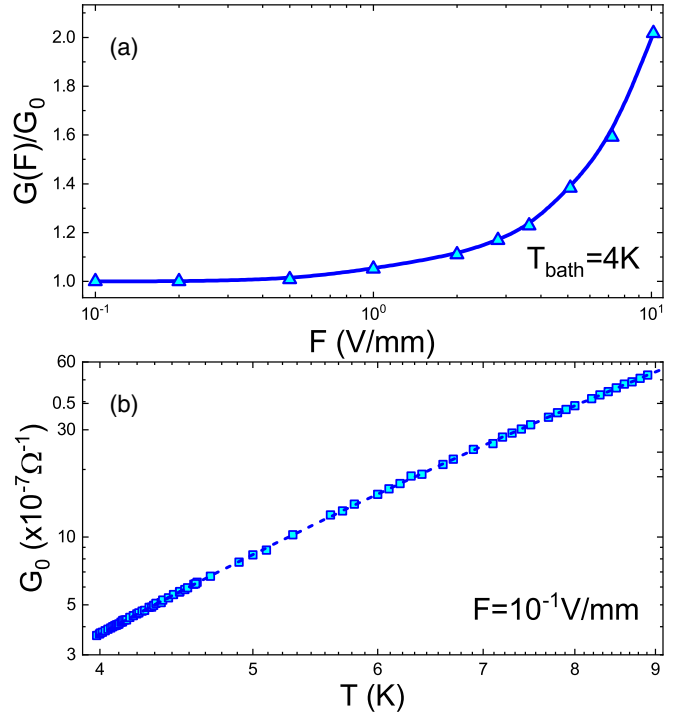


FIG. 2. Pertinent transport data taken for the sample. (a) The relative change of conductance as function of the applied electric field. (b) The conductance vs bath temperature of the sample measured by two-terminal ac technique using a bias voltage in the linear-response regime at a frequency $f = 73$ Hz. At each point, the sample was allowed to relax for 1–2 h to ensure steady-state conditions. The dashed line is a fit to $G_0(T) \propto \exp[-(T_0/T)^{1/3}]$ with $T_0 \simeq 5800$ K.

that fulfills $\eta(T_{\text{eff}}) = \eta(T)$ as illustrated in Fig. 5 for a specific η value (red arrow). This allows a direct comparison between the $T_{\text{eff}}(F)$ of the two thermometers depicted in Fig. 6.

It is not surprising that thermometer 1 agrees with thermometer 2 *only* when F is vanishingly small. It is however remarkable that the largest relative discrepancy between

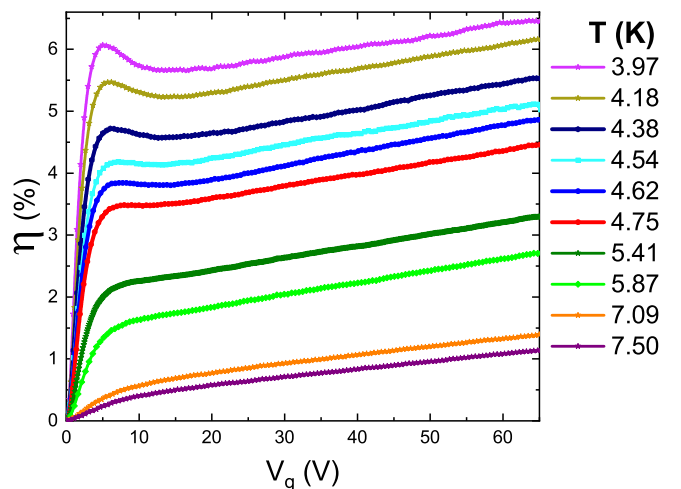


FIG. 3. Conductance vs gate voltage $G(V_g)$ for the In_xO film. Curves were taken at indicated temperatures with the same sweep rate: $\partial V_g/\partial t = 1.2$ V/s.

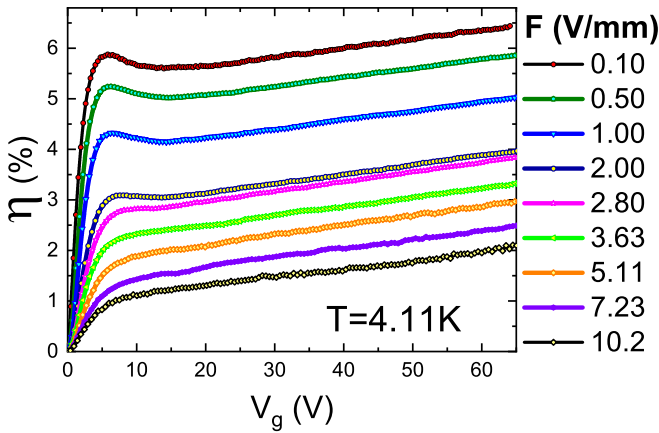


FIG. 4. Same as in Fig. 3 except that the $G(V_g)$ curves were taken under various electric fields.

the thermometers is where the system is just off the linear response regime in terms of $G_0(F)$. This observation demonstrates that T_{eff} may be an ill-defined concept in a nonequilibrium steady state, even under a fairly weak drive. Such hot-electron effects [19] are commonly manifested in the transport studies of semiconductors driven by non-Ohmic fields. The system conductance under these conditions may also be influenced by electron-electron correlations.

The difference between the two thermometers is probably even larger than conveyed by Fig. 6. Note that T_{eff} for thermometer 1 is determined here solely on the basis of the measured $\Delta G(F)$. However, $\Delta G(F)$ is composed of *two* contributions. The first is due to field-assisted tunneling [20–23], the second results from joule heating [24–26]. The T_{eff} used in Fig. 6 is therefore larger than the value based on assuming just

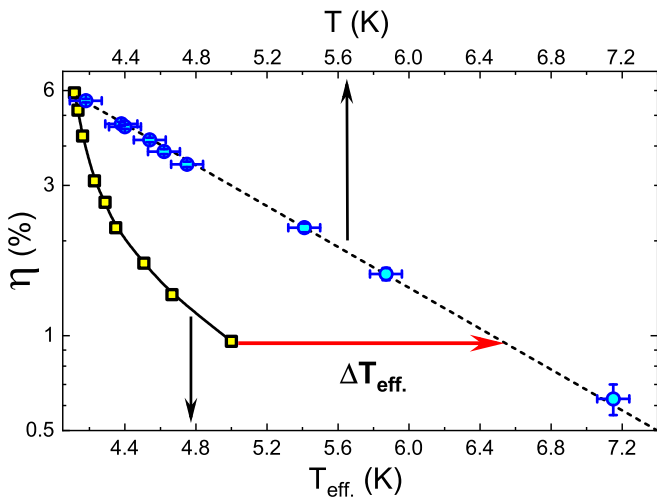


FIG. 5. Contrasting the effective temperatures yielded by the two thermometers under applied fields. Data for T_{eff} for thermometer 1 (squares, and line as a guide to the eye). Each η taken from Fig. 4 is assigned a T_{eff} by using the data in Fig. 2 for $G(T)$ and $G(F)$ for the sample. Mapping T_{eff} for thermometer 2 is accomplished by matching the value of the measured η with the equilibrium values for $\eta(T)$ taken from Fig. 3. The dashed line is a fit to $\eta \propto \exp[-T/T^*]$ with $T^* = 1.34$.

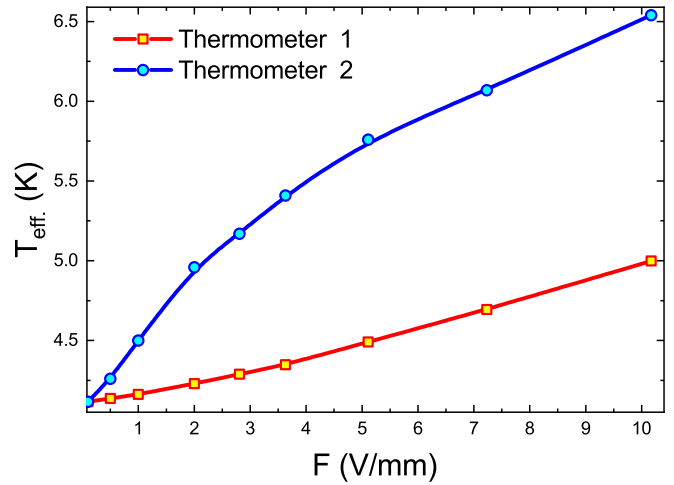


FIG. 6. Direct comparison of the effective temperatures for thermometers 1 and 2 based on data from Fig. 5 (see text).

heating. This complication, in different forms, is inherent to resistance-based thermometry commonly used in experiments on disordered insulators.

Moreover, when the system is driven into a NESS by exposure to IR illumination the discrepancy between the two T_{eff} 's turns out to be significantly larger than under non-Ohmic fields. Figure 7(a) shows the raw data for the equilibrium $G(V_g)$ compared with a trace taken under weak IR illumination. Note first that the zero-bias conductance of the sample

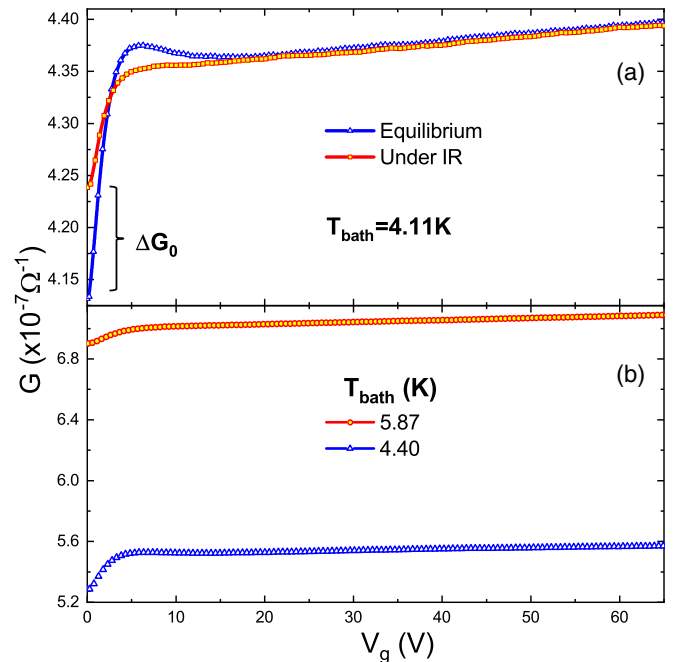


FIG. 7. Conductance versus gate voltage $G(V_g)$ for the In_xO sample under two different conditions. (a) Comparing $G(V_g)$ measured at equilibrium with a trace measured under IR illumination. The IR source (operating at $0.2 \mu\text{A}$ while biased at 1.003 V) has been on for 75 min before the trace was taken to ensure steady-state conditions. (b) $G(V_g)$ traces taken from the (equilibrium) data in Fig. 3 as a pair that exhibit values of η similar to these of the traces in (a).

has slightly increased in the NESS of the sample by ΔG_0 , a relative change of $\approx 2.5\%$. This is equivalent (using the calibration graph in Fig. 2) to $\Delta T \approx 24$ mK, while (using the data in Fig. 5) the change in η is equivalent to $\Delta T_{\text{eff}} \approx 1.1$ K.

Secondly, to get a comparable shift of ΔT_{eff} requires an applied non-Ohmic field $F \approx 3.7$ V/mm that, in turn, entails maintaining input power into the sample of the order of 10^{-5} W. The *total* power used by the light-emitting diode in Fig. 7(a) is $\approx 10^{-7}$ W [27]. Obviously much less power is required by IR illumination to reduce η than by applying low frequency fields.

Another intriguing feature of the NESS maintained by IR illumination may be appreciated by comparing the data in Fig. 7(a) with Fig. 7(b). The latter illustrates characteristic $G(V_g)$ traces of the electron glass measured in *equilibrium*. As the bath temperature is raised, or when a larger non-Ohmic F is applied, the *entire* $G(V_g)$ trace is shifted to higher values. By contrast, only G_0 is enhanced when the sample is exposed to IR while, for $V_g \geq 2$ V, $G(V_g)$ falls below the equilibrium value. This feature was consistently observed on three other samples using IR power $\lesssim 10^{-6}$ W.

To all appearances, the difference between the two NESS protocols depends on the nature of the drive: non-Ohmic field versus IR excitation.

The natural question is what makes IR illumination so effective in reducing η while barely affecting the system conductance? Additionally, why does the NESS created by non-Ohmic fields require much larger power to achieve a similar reduction in η ?

The answer to both questions is related to the way the invested power of a protocol modifies the phonon distribution $D(\varepsilon)$ of the system. In equilibrium, $D(\varepsilon)$ is given by the Bose-Einstein distribution that, at cryogenic temperatures, means an abundance of low-frequency phonons and exponentially rare high-frequency ones.

Applying non-Ohmic fields F mostly adds low-frequency modes to the spectrum. Down-going transitions associated with hopping under such fields produce athermal phonons in the spectrum but with energies up to $\approx eFL$, where $L_C = L_C(F, T)$ is the percolation radius [24,25,28,29]. At typical values for $L_C \approx 10^{-7}$ m at $T \approx 4$ K, and fields in the range used in this work, the energy accumulated from the field will appear as an excess of phonons at a few degrees above the bath temperature.

When the system is exposed to the IR source the modification to $D(\varepsilon)$ is more profound. The IR initiates a cascade process: electrons are excited to high energy and then relax by phonon emission [30]. The NESS that sets in sustains

vibrations at phonon energies of few hundred degrees [31]. Then, it is the high-energy part of $D(\varepsilon)$ that is significantly boosted, while the relative change in the low-energy phonon bank is small. The greater efficiency of the IR protocol relative to that of non-Ohmic fields in reducing η is a consequence of the excess high-energy modes it creates. These modes allow transitions that, in equilibrium, would occur only at temperatures of few hundred degrees where no memory dip has ever been observed in any of the half dozen [18] electron glasses measured to date.

The two thermometers also differ in the typical energy controlling their response. For thermometer 1 (based on the measured conductance), this is the optimal hopping energy [32,33] $E_{\text{opt}} = (k_B T)^{2/3} (\partial n / \partial \mu d \xi^2)^{-1/3}$. Here, $\partial n / \partial \mu \approx 10^{32} \text{ erg}^{-1} \text{ cm}^{-3}$ is the density of states, d is the film thickness, and $\xi \approx 5$ nm is the localization length [estimated from $G(T)$ in Fig. 2(b)]. With these values E_{opt} is of order ≈ 1 meV at ≈ 5 K. The characteristic energy for thermometer 2 is the disorder energy $W \gtrsim 0.4$ eV. This is estimated on the basis of the condition that W is large enough to Anderson localize the system and to slow its relaxation such that the memory dip is resolved in the field-effect scans [18].

Hopping conductivity takes place in a current-carrying network (CNN) utilizing regions of the relatively weak disorder. The CNN encompasses regions of the highest disorder in the sample [28,29,34]. The large disorder in these regions is responsible for the slow relaxation of the electron glass [18]. The two regions [35] communicate mainly via low-energy phonons [18], and electron-electron interaction. The range over which interaction is effective however may depend on available resonances and therefore on quantum coherence in the medium [36].

In sum, we have demonstrated that driving an Anderson insulator even slightly out of its linear response entails a sharp thermometers conflict, suggesting that thermometry in this regime [37] should be treated with some doubt. The frequency of the drive turns out to be a pivotal parameter in the thermometer's discrepancy. Explicitly, the difference between the thermometers is significantly larger when the drive initiates high-frequency energy quanta in the medium as occurs in the IR protocol. A specific reason for this was offered based on the quantum nature of the phonon energy distribution. Phonons are an essential ingredient in establishing steady-state conditions in these NESS experiments. Our results show that they also play a nontrivial role in nonequilibrium phenomena.

The author thanks P. Bhandari, V. Malik, and M. Schechter for illuminating discussions on their simulation work.

- [1] G. Tripathy and M. Barma, Steady state and dynamics of driven diffusive systems with quenched disorder, *Phys. Rev. Lett.* **78**, 3039 (1997).
- [2] L. Balents, M. C. Marchetti, and L. Radzihovsky, Nonequilibrium steady states of driven periodic media, *Phys. Rev. B* **57**, 7705 (1998).
- [3] F.-J. Pérez-Reche, L. Truskinovsky, and G. Zanzotto, Driving-induced crossover: From classical criticality to self-organized criticality, *Phys. Rev. Lett.* **101**, 230601 (2008).

- [4] A. Janot, T. Hyart, P. R. Eastham, and B. Rosenow, Superfluid stiffness of a driven dissipative condensate with disorder, *Phys. Rev. Lett.* **111**, 230403 (2013).
- [5] H. Ikeda and Y. Kuroda, Does spontaneous symmetry breaking occur in periodically driven low-dimensional non-equilibrium classical systems? [arXiv:2304.14235v1](https://arxiv.org/abs/2304.14235v1).
- [6] M. S. Rudner and N. H. Lindner, Band structure engineering and non-equilibrium dynamics in floquet topological insulators, *Nat. Rev. Phys.* **2**, 229 (2020).

- [7] M. Caravaca, A. M. Somoza, and M. Ortuño, Nonlinear conductivity of two-dimensional Coulomb glasses, *Phys. Rev. B* **82**, 134204 (2010).
- [8] P. Bhandari, V. Malik, and M. Schechter, Variable range hopping in a non-equilibrium steady state, *Phys. Rev. B* **108**, 024203 (2023).
- [9] J. H. Davies, P. A. Lee, and T. M. Rice, Electron glass, *Phys. Rev. Lett.* **49**, 758 (1982); M. Pollak, M. Ortuño, and A. Frydman, *The Electron Glass* (Cambridge University Press, Cambridge, England, 2013).
- [10] G. Vignale, Quantum electron glass, *Phys. Rev. B* **36**, 8192 (1987).
- [11] Z. Ovadyahu and M. Pollak, Disorder and magnetic field dependence of slow electronic relaxation, *Phys. Rev. Lett.* **79**, 459 (1997).
- [12] C. C. Yu, Time-dependent development of the Coulomb gap, *Phys. Rev. Lett.* **82**, 4074 (1999).
- [13] M. Müller and L. B. Ioffe, Glass transition and the Coulomb gap in electron glasses, *Phys. Rev. Lett.* **93**, 256403 (2004).
- [14] E. Lebanon and M. Müller, Memory effect in electron glasses: Theoretical analysis via a percolation approach, *Phys. Rev. B* **72**, 174202 (2005).
- [15] V. Malik and D. Kumar, Formation of the Coulomb gap in a Coulomb glass, *Phys. Rev. B* **69**, 153103 (2004).
- [16] A. Amir, Y. Oreg, and Y. Imry, Mean-field model for electron-glass dynamics, *Phys. Rev. B* **77**, 165207 (2008); Electron glass dynamics, *Annu. Rev. Condens. Matter Phys.* **2**, 235 (2011).
- [17] Y. Meroz, Y. Oreg, and Y. Imry, Memory effects in the electron glass, *Europhys. Lett.* **105**, 37010 (2014).
- [18] Z. Ovadyahu, Slow dynamics of the electron-glasses: The role of disorder, *Phys. Rev. B* **95**, 134203 (2017).
- [19] P. Kleinert, Theory of hot-electron quantum diffusion in semiconductors, *Phys. Rep.* **485**, 1 (2010) and references therein.
- [20] R. M. Hill, Hopping conduction in amorphous solids, *Philos. Mag.* **24**, 1307 (1971).
- [21] N. Apsley and H. P. Hughes, Temperature-and field-dependence of hopping conduction in disordered systems, II, *Philos. Mag.* **31**, 1327 (1975).
- [22] M. Pollak and I. Riess, A percolation treatment of high-field hopping transport, *J. Phys. C* **9**, 2339 (1976).
- [23] B. I. Shklovskii, *Fiz. Tekh. Poluprovodn.* **6**, 2335 (1972) [Hopping conduction in semiconductors subjected to a strong electric field, *Sov. Phys. Semicond.* **6**, 1964 (1973)].
- [24] N. Markovic, C. Christiansen, D. E. Grupp, A. M. Mack, G. Martinez-Arizala, and A. M. Goldman, Anomalous hopping exponents of ultrathin metal films, *Phys. Rev. B* **62**, 2195 (2000).
- [25] V. Orlyanchik and Z. Ovadyahu, Conductance noise in interacting Anderson insulators driven far from equilibrium, *Phys. Rev. B* **72**, 024211 (2005).
- [26] Y. Yuzhelevski, V. Markovich, V. Dikovskiy, E. Rozenberg, G. Gorodetsky, G. Jung, D. A. Shulyatev, and Ya. M. Mukovskii, Current-induced metastable resistive states with memory in low-doped manganites, *Phys. Rev. B* **64**, 224428 (2001).
- [27] Note that only part of this power is actually invested in the sample due to imperfect efficiency, optical absorption, beam-geometry, etc.
- [28] V. Ambegaokar, B. I. Halperin, and J. S. Langer, Hopping conductivity in disordered systems, *Phys. Rev. B* **4**, 2612 (1971).
- [29] M. Pollak, A percolation treatment of dc hopping conduction, *J. Non-Cryst. Solids* **11**, 1 (1972).
- [30] Z. Ovadyahu, Optical excitation of electron glasses, *Phys. Rev. B* **83**, 235126 (2011).
- [31] Z. Ovadyahu, Some finite temperature aspects of the Anderson transition, *J. Phys. C* **19**, 5187 (1986).
- [32] N. F. Mott and G. A. Davis, *Electronic Processes in Non-Crystalline Materials*, 2nd ed. (Clarendon Press, Oxford, 1979).
- [33] B. I. Shklovskii and A. L. Efros, in *Electronic Properties of Doped Semiconductors* (Springer-Verlag, Berlin, 1984).
- [34] C. H. Seager and G. E. Pike, Percolation and conductivity: A computer study. I, *Phys. Rev. B* **10**, 1435 (1974).
- [35] The spatial scale associated with the inhomogeneity is the percolation radius L_C , which, at cryogenic temperatures, is typically $\simeq 50N^{-1/3}$ [24,32]. To capture the dichotomy between conductance and relaxation the simulation ought to include samples sizes considerably larger than L_C , a tall task by today's standards.
- [36] J. B. Pendry, Quasi-extended electron states in strongly disordered systems, *J. Phys. C: Solid State Phys.* **20**, 733 (1987); Z. Ovadyahu, Long-range influence of manipulating disordered-insulators locally, *Phys. Rev. B* **101**, 094202 (2020); Suppressing quantum effects by optically driven nonequilibrium phonons, **103**, L100206 (2021).
- [37] M. Ovadia, B. Sacépé, and D. Shahar, Electron-phonon decoupling in disordered insulators, *Phys. Rev. Lett.* **102**, 176802 (2009); B. L. Altshuler, V. E. Kravtsov, I. V. Lerner, and I. L. Aleiner, Jumps in current-voltage characteristics in disordered films, *ibid.* **102**, 176803 (2009).